Taylor & Francis
Taylor & Francis Group

Automatika

Journal for Control, Measurement, Electronics, Computing and Communications

ISSN: (Print) (Online) Journal homepage: https://www.tandfonline.com/loi/taut20

Active vehicle obstacle avoidance based on integrated horizontal and vertical control strategy

Xu Li , Yibo Yang & Jianchun Wang

To cite this article: Xu Li , Yibo Yang & Jianchun Wang (2020) Active vehicle obstacle avoidance based on integrated horizontal and vertical control strategy, Automatika, 61:3, 448-460, DOI: 10.1080/00051144.2020.1778215

To link to this article: https://doi.org/10.1080/00051144.2020.1778215

Published online: 15 Jun 2020.

AUTOMATIKA
2020, VOL. 61, NO. 3, 448–460
https://doi.org/10.1080/00051144.2020.1778215

REGULAR PAPER

OPEN ACCESS Check for updates

Active vehicle obstacle avoidance based on integrated horizontal and vertical control strategy

Xu Li, Yibo Yang and Jianchun Wang

School of Transportation, Shandong University of Science and Technology, Qingdao, People's Republic of China

ABSTRACT

In this paper, an integrated control method is proposed which is based on a planning of vehicle's path and speed with respect to obstacles and a model predictive control for tracking this path. The planning layer builds a model predictive control framework based on the vehicle kinematics model; based on the potential field theory, comprehensively considers the vehicle's state information and the relative position and velocity information of the obstacles, establishes the potential field function, introduces the optimization objective function, and optimizes vehicle's path and speed. The tracking layer builds a model predictive control framework based on the vehicle dynamics model, establishes an optimized objective function that takes the optimal front wheel rotation angle and optimal longitudinal acceleration as inputs, and constrains the lateral acceleration and yaw angular velocity to achieve the vehicle's obstacle avoidance path track. A co-simulation platform of CarSim and Matlab/Simulink was built to analyse the performance of the vehicle under static and dynamic obstacles under different initial speed conditions. The results show that the vehicle can track the reference path and reference speed smoothly, realize the horizontal and vertical comprehensive control of active obstacle avoidance, and verify the effectiveness of the proposed control method.

ARTICLE HISTORY
Received 11 October 2019
Accepted 14 April 2020

KEYWORDS
Automotive engineering; active obstacle avoidance; model predictive control; intelligent vehicle; integrated path and speed planning; horizontal and vertical integrated control

Nomenclature

$\{XYZ\}$	The global coordinate system
$\{xyz\}$	The vehicle coordinate system
a_x	The vehicle longitudinal acceleration
a_y	The vehicle lateral acceleration
v_x	The vehicle longitudinal speed
v_y	The vehicle lateral speed
θ	The vehicle heading angle
φ	The vehicle yaw angle
ω	The vehicle yaw rate
δ_f	The front wheel angle
I_z	The yaw moment of inertia vehicle
m	The total mass of vehicle
a	The distance from the centre of mass to the front axle
b	The distance from the centre of mass to the rear axle
F_{lf}	The longitudinal force of the front axle
F_{lr}	The longitudinal force of the rear axle
F_{cf}	The lateral force of the front axle
F_{cr}	The lateral force of the rear axle
α_f	The front tire side yaw angle
α_r	The rear tire side yaw angle
C_{cf}	The front tire cornering stiffness
C_{cr}	The rear tire cornering stiffness
g	The gravity acceleration

1. Introduction

Active obstacle avoidance has always been a hot issue in autonomous driving, and its reliability is directly related to users' recognition of autonomous driving. Active obstacle avoidance as one of the key technologies for autonomous vehicles has attracted wide attention [1–6]. Moreover, only by increasing people's recognition of autonomous driving, the rapid development of self-driving cars be promoted. However, the research on the active obstacle avoidance problem mainly focuses on the emergency steering and the active steering obstacle avoidance under the uniform speed condition, and the horizontal and vertical control of the vehicle is less comprehensively considered to realize the active obstacle avoidance of intelligent vehicle.

In recent years, many scholars have carried out step-by-step research on the active obstacle avoidance of intelligent vehicles in accordance with the simple and comprehensive, single-to-all research methods. Choe TS et al. [7] proposed a steering potential field to modify the traditional artificial potential field, and based on the obstacle information to establish the obstacle repulsion potential field, the speed, steering and braking of the intelligent vehicle under the joint action of the two virtual potential fields. The instructions are corrected to guide the vehicle along the ideal path.

CONTACT Jianchun Wang wjceq@126.com

Moon et al. [8] comprehensively consider the location, speed and direction of intelligent vehicles, and proposed a method to find a reasonable path in unknown obstacles based on artificial potential field theory, which can effectively perform real-time obstacle avoidance. Tomas-Gbarron et al. [9] analysed the obstacle avoidance problem of autonomous vehicles under high-speed conditions and transformed them into multi-objective optimization problems, and optimized the vehicle travel path by weighted aggregation. Wang et al. [10] proposed a driving safety potential field model based on potential field theory, including static obstacle potential field, dynamic obstacle potential field, driver behaviour potential field, and finally realized intelligent vehicle based on driving safety potential field model along with route plan. Cao et al. [11] designed a potential field model in the form of harmonic function according to the characteristics of obstacles, road boundaries and target points, and obtained the optimal path by gradient descent method.

In recent years, with increasing number of studies, the model predictive control method, which is one of the advanced control methods in the industrial field, has been gradually applied to the research of intelligent driving, and has achieved fruitful results. Mousavi et al. [12] introduced obstacles and road structures into the model predictive control in the form of constraints to achieve obstacle avoidance. Rosolia et al. [13] constructed a two-layer obstacle avoidance control framework. The upper layer uses nonlinear model predictive control method for obstacle avoidance planning, and the lower layer uses preview-based linear feedback control method. Ji et al. [14] proposed a path planning and tracking framework. The planning layer establishes a dangerous potential field including roads and obstacles. When an intelligent vehicle collides with an obstacle, an obstacle avoidance path is generated. The tracking layer is based on model prediction control calculation. The front wheel corners enable the vehicle to track the collision avoidance path. Zhu et al. [15] proposed an intelligent vehicle speed tracking control method based on model predictive control (MPC) framework, and realized driving or braking control through a non-calibrated switching algorithm, which was verified by simulation and real vehicle test. This method accurately tracks speed. Huang et al. [16] proposed a model prediction controller based on potential field theory for the first time, which has the functions of path planning and tracking control. However, the study uses a relatively simple vehicle kinematics model, and its tracking control accuracy needs to be further improved.

In summary, most active obstacle avoidance studies do not consider the horizontal and vertical integrated control of intelligent vehicles in the process of obstacle avoidance. In the actual driving process, only a single steering or braking is used to achieve active obstacle avoidance of the vehicle. It is not enough to change the longitudinal speed of the vehicle through the necessary acceleration or braking, so that the vehicle can better adapt to different road conditions; in addition, the description of the collision of dynamic obstacles is not precise enough, and it is too simple to describe by being a constraint. In this paper, considering the horizontal and vertical control of the vehicle and the relative state information of the vehicle and the obstacle, a comprehensive control method based on the model predictive control theory for integrated path and speed integrated planning and tracking is proposed.

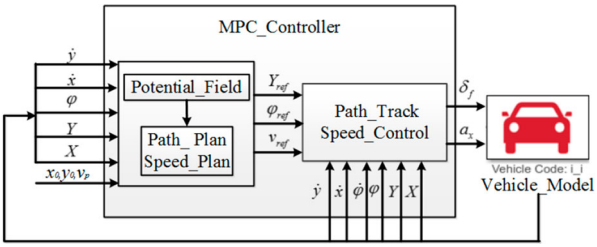

Figure 1. Block diagram of intelligent vehicle active obstacle avoidance control system.

The control block diagram for the active obstacle avoidance of intelligent vehicles, proposed in this paper as shown in Figure 1. The intelligent vehicle active obstacle avoidance control framework mainly includes three parts: planning layer (path planning, speed planning), tracking layer (path tracking, speed tracking), and execution layer (replaced by CarSim virtual vehicle). The planning layer obtains the reference speed control model based on the sensor's motion state information. The relative position and velocity information of the vehicle and the obstacle. Based on the potential field theory, the corresponding gravitational field function and the repulsive field functions are established and based on the fifth-order polynomial programming. The tracking layer tracks the reference path and reference speed planned by the planning layer based on the nonlinear vehicle dynamics model, and outputs the optimal front wheel angle and longitudinal acceleration to the execution layer vehicle model, thereby achieving smooth active obstacle avoidance.

2. Planning controller design

Aiming at complex operating environment of intelligent vehicles, the integrated path and speed planning controller based on artificial potential field theory and model predictive control idea is designed to provide accurate horizontal and vertical control planning for vehicle active obstacle avoidance, and to improve the mobility of vehicle control and vehicle stability.

2.1. *Vehicle kinematics model*

In order to reduce the calculation of planning layer and improve the efficiency of solving, the vehicle is

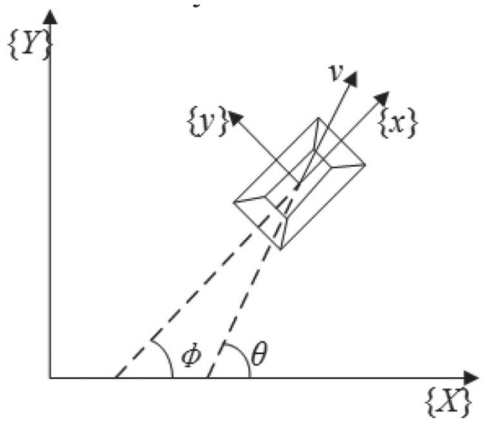

Figure 2. Simplified diagram of vehicle kinematics model.

simplified into a rigid body model, and a rigid body plane motion model is established, as shown in Figure 2, *XOY* is the global coordinate system and *xoy* is the vehicle coordinate system.

According to the simplified diagram of the vehicle kinematics model, the vehicle kinematics model can be described as follows:

$$\begin{aligned}\ddot{y} &= a_y \\ \ddot{x} &= a_x \\ \dot{\theta} &= \frac{a_y}{\dot{x}} \\ \dot{X} &= \dot{x}\cos\varphi - \dot{y}\sin\varphi \\ \dot{Y} &= \dot{x}\sin\varphi + \dot{y}\cos\varphi \end{aligned} \tag{1}$$

The $\ddot{x}$ and $\ddot{y}$ are the vehicle's longitudinal acceleration and lateral acceleration, respectively; φ is the vehicle yaw angle, that is, the angle between the vehicle coordinate system *ox* axis and the global coordinate system *OX* axis; θ is the vehicle heading angle, that is, the angle between the vehicle's centroid speed and the global coordinate system *OX* axis; $\dot{X}$ and $\dot{Y}$ are the longitudinal and lateral speeds of the vehicle in the global coordinate system, respectively. When the vehicle is travelling at a high speed, the lateral speed of the vehicle is much smaller than the longitudinal speed, so $\theta = \varphi$ is assumed.

According to the state space system, state variables are selected: $\boldsymbol{X} = \begin{bmatrix}\dot{y} & \dot{x} & \varphi & Y & X\end{bmatrix}^{\mathrm{T}}$, control input $\boldsymbol{\chi} = \begin{bmatrix}a_y & a_x\end{bmatrix}^{\mathrm{T}}$, control output $\boldsymbol{Y} = \begin{bmatrix}Y & \varphi & \dot{x}\end{bmatrix}^{\mathrm{T}}$, the equation of state is

$$\begin{aligned}\dot{\boldsymbol{X}} &= f(\boldsymbol{X}, \boldsymbol{\chi}) \\ \boldsymbol{Y} &= g(\boldsymbol{X})\end{aligned} \tag{2}$$

Equation (2) is a continuous nonlinear state equation. To design a model prediction controller, a nonlinear continuous system must be transformed into a linear discrete system. Therefore, Taylor expansion is performed at X_0, χ_0 and high-order terms are ignored, the equation is obtained as:

$$\begin{aligned}\dot{\boldsymbol{X}} = f(\boldsymbol{X}_0, \boldsymbol{\chi}_0) &+ \underbrace{\left[\frac{\partial f}{\partial \boldsymbol{X}}\Big|_{\boldsymbol{X}_0, \boldsymbol{\chi}_0}\right]}_{J(\boldsymbol{X})}(\boldsymbol{X} - \boldsymbol{X}_0) \\ &+ \underbrace{\left[\frac{\partial f}{\partial \boldsymbol{\chi}}\Big|_{\boldsymbol{X}_0, \boldsymbol{\chi}_0}\right]}_{J(\boldsymbol{\chi})}(\boldsymbol{\chi} - \boldsymbol{\chi}_0)\end{aligned} \tag{3}$$

where $J(X)$, $J(\chi)$ are $f(X, \chi)$ for the state variable and the Jacobian matrix of the control input variable. Therefore, the original model is linearized as:

$$\begin{aligned}\dot{\tilde{\boldsymbol{X}}} &= \boldsymbol{A}_c\tilde{\boldsymbol{X}} + \boldsymbol{B}_c\tilde{\boldsymbol{\chi}} \\ \tilde{\boldsymbol{Y}} &= \boldsymbol{C}_c\tilde{\boldsymbol{X}}\end{aligned} \tag{4}$$

Among them: $\tilde{\boldsymbol{X}} = \boldsymbol{X} - \boldsymbol{X}_0$, $\tilde{\boldsymbol{\chi}} = \boldsymbol{\chi} - \boldsymbol{\chi}_0$, $\boldsymbol{A}_c = \boldsymbol{J}(\boldsymbol{X})$, $\boldsymbol{B}_c = \boldsymbol{J}(\boldsymbol{\chi})$,

$$\boldsymbol{C}_c = \begin{bmatrix}0 & 0 & 0 & 1 & 0 \\ 0 & 0 & 1 & 0 & 0 \\ 0 & 1 & 0 & 0 & 0\end{bmatrix}^{\mathrm{T}}$$

The linear model is discretized by the first-order difference quotient method, and the discrete state space equation is obtained:

$$\begin{aligned}\tilde{\boldsymbol{X}}(k+1) &= \tilde{\boldsymbol{A}}_{\boldsymbol{c}}\tilde{\boldsymbol{X}}(k) + \tilde{\boldsymbol{A}}_{\boldsymbol{c}}\tilde{\boldsymbol{\chi}}(k) \\ \tilde{\boldsymbol{Y}}(k) &= \boldsymbol{C}_c\tilde{\boldsymbol{X}}(k)\end{aligned} \tag{5}$$

Among them: $\tilde{\boldsymbol{A}}_{\boldsymbol{c}} = \boldsymbol{I} + T\boldsymbol{A}_c$, $\tilde{\boldsymbol{B}}_{\boldsymbol{c}} = T\boldsymbol{B}_c$. Afterwards,

$$\boldsymbol{X}(k|t) = \begin{bmatrix}\tilde{\boldsymbol{X}}(k|t) \\ \tilde{\boldsymbol{\chi}}(k-1|t)\end{bmatrix} \tag{6}$$

New state space equation is obtained as:

$$\begin{aligned}\boldsymbol{X}(k+1|t) &= \boldsymbol{A}_d\boldsymbol{X}(k|t) + \boldsymbol{B}_d\Delta\boldsymbol{u}(k) \\ \boldsymbol{\eta}(k|t) &= \boldsymbol{C}_d\boldsymbol{X}(k|t)\end{aligned} \tag{7}$$

Among them:

$$\boldsymbol{A}_d = \begin{bmatrix}\tilde{\boldsymbol{A}}_{\boldsymbol{c}} & \tilde{\boldsymbol{B}}_{\boldsymbol{c}} \\ \boldsymbol{0}_{2\times5} & \boldsymbol{I}_2\end{bmatrix}, \boldsymbol{B}_d = \begin{bmatrix}\tilde{\boldsymbol{B}}_{\boldsymbol{c}} \\ \boldsymbol{I}_2\end{bmatrix}, \boldsymbol{C}_d = \begin{bmatrix}\boldsymbol{C}_c & \boldsymbol{0}_{3\times2}\end{bmatrix}$$

According to the theory of model predictive control, n_p is defined as the prediction time domain, n_c as the control time domain, and $n_c \leq n_p$, then the system predictive output and the current state of the system in the

whole prediction range. The relationship is

$$\boldsymbol{Y}(N_p) = \boldsymbol{\Psi}_k \boldsymbol{X}(k) + \boldsymbol{\Theta}_k \boldsymbol{\chi}(k) \tag{8}$$

The state matrix and the control matrix are:

$$\boldsymbol{\Psi}_k = \begin{bmatrix} \boldsymbol{C}_d\boldsymbol{A}_d & \boldsymbol{C}_d\boldsymbol{A}_d^2 & \cdots & \boldsymbol{C}_d\boldsymbol{A}_d^{N_c} & \cdots & \boldsymbol{C}_d\boldsymbol{A}_d^{N_p} \end{bmatrix}^{\mathrm{T}} \tag{9}$$

$$\boldsymbol{\Theta}_k = \begin{bmatrix} \boldsymbol{C}_d\boldsymbol{B}_d & 0 \\ \boldsymbol{C}_d\boldsymbol{A}_d\boldsymbol{B}_d & \boldsymbol{C}_d\boldsymbol{B}_d \\ \vdots & \vdots \\ \boldsymbol{C}_d\boldsymbol{A}_c^{N_c-1}\boldsymbol{B}_d & \boldsymbol{C}_d\boldsymbol{A}_c^{N_c-2}\boldsymbol{B}_d \\ \boldsymbol{C}_d\boldsymbol{A}_c^{N_c}\boldsymbol{B}_d & \boldsymbol{C}_d\boldsymbol{A}_c^{N_c-1}\boldsymbol{B}_d \\ \vdots & \vdots \\ \boldsymbol{C}_d\boldsymbol{A}_c^{N_p-1}\boldsymbol{B}_d & \boldsymbol{C}_d\boldsymbol{A}_c^{N_p-2}\boldsymbol{B}_d \end{bmatrix} \begin{matrix} 0 & 0 \\ \cdots & 0 \\ \ddots & \vdots \\ \cdots & \boldsymbol{C}_d\boldsymbol{B}_d \\ \cdots & \boldsymbol{C}_d\boldsymbol{A}_d\boldsymbol{B}_d \\ \ddots & \vdots \\ \cdots & \boldsymbol{C}_d\boldsymbol{A}_c^{N_p-N_c-1}\boldsymbol{B}_d \end{matrix} \tag{10}$$

The system predictive output matrix is

$$\boldsymbol{Y}(N_p) = \begin{bmatrix} \boldsymbol{\eta}(k+1|k) \\ \boldsymbol{\eta}(k+2|k) \\ \vdots \\ \boldsymbol{\eta}(k+N_c|k) \\ \vdots \\ \boldsymbol{\eta}(k+N_p|k) \end{bmatrix} \tag{11}$$

2.2. Obstacle avoidance objective function

In the autonomous obstacle avoidance control of intelligent vehicles, the main purpose is to achieve the obstacle avoidance while tracking the global reference path as accurately as possible. Secondly, to improve the stability of the intelligent vehicle in the obstacle avoidance process, thereby improving the passenger ride comfort. Based on the artificial potential field theory, the corresponding gravitational field function $J_{\mathrm{pos},i}$ and the repulsive field function $J_{\mathrm{obs},i}$ are established. The two potential field functions are as follows:

$$J_{\mathrm{pos},i} = Q_\eta(\eta_i - \eta_{\mathrm{ref}})^2 + R_u(u_i)^2 \tag{12}$$

$$J_{\mathrm{obs},i} = \frac{S_{\mathrm{obs}} v_{r,i}}{(x_i - x_0)^2 + (y_i - y_0)^2 + \varepsilon} \tag{13}$$

where Q_η, R_u are the two weight coefficients of the gravitational field function, which represent the weights of two different gravitational sources; S_{obs} is the weight coefficient of the repulsive field function. The larger the value, the more conservative the obstacle avoidance planning result; $v_{r,i}$ is the relative speed of the vehicle and the obstacle; (x_i, y_i) is the predicted position coordinate of the intelligent vehicle in the i-th step; (x_0, y_0) is the global position coordinate of the obstacle; ε is the correction factor of the repulsive field function, which is a very small positive value, preventing the phenomenon of infinite repulsive force.

Therefore, the total potential energy J in the autonomous obstacle avoidance process of the smart vehicle can be obtained, as shown in the following formula (14).

$$J = \sum_{i=1}^{N_p} (J_{\mathrm{pos},i} + J_{\mathrm{obs},i}) \tag{14}$$

In addition, the repulsion potential energy maps with relative velocities of 5 and 10 m/s are shown in Figure 3.

In order to ensure the feasibility of local path planning, the optimization control input a_x, a_y and its rate of change must be constrained. According to the existing theoretical knowledge on automobiles and related literature, combined with the actual vehicle test, it can be known that:

$$-0.9\mathrm{g} \le a_x \le 0.6\mathrm{g}$$
$$-0.4\mathrm{g} \le a_y \le 0.4\mathrm{g} \tag{15}$$
$$-2\mathrm{g/s} \le \Delta a_x \le 2\mathrm{g/s}$$
$$-2\mathrm{g/s} \le \Delta a_y \le 2\mathrm{g/s} \tag{16}$$

Combined with the total potential energy and the corresponding constraints, the obstacle avoidance path planning of the intelligent vehicle can be transformed into an optimization problem as shown in the following equation:

$$\begin{aligned} &\min_{\chi} \boldsymbol{J} \\ &\text{s.t.} \boldsymbol{\chi}_{\min} \le \boldsymbol{\chi} \le \boldsymbol{\chi}_{\max} \\ &\Delta\boldsymbol{\chi}_{\min} \le \Delta\boldsymbol{\chi} \le \Delta\boldsymbol{\chi}_{\max} \end{aligned} \tag{17}$$

where $\chi_{\min}$ and $\chi_{\max}$ are the minimum and maximum set of control input quantities respectively; $\Delta\chi_{\min}$ and $\Delta\chi_{\max}$ are the minimum and maximum set of control input increments, respectively.

2.3. Local planning path

According to a large number of studies on driver's steering obstacle avoidance behaviour, the driving path of the vehicle in the process of obstacle avoidance is similar to a five-order polynomial curve [17,18]. The obstacle avoidance route formed by the fifth-order polynomial fitting function can make the displacement, velocity and acceleration curve of the intelligent vehicle in the obstacle avoidance process continuous and

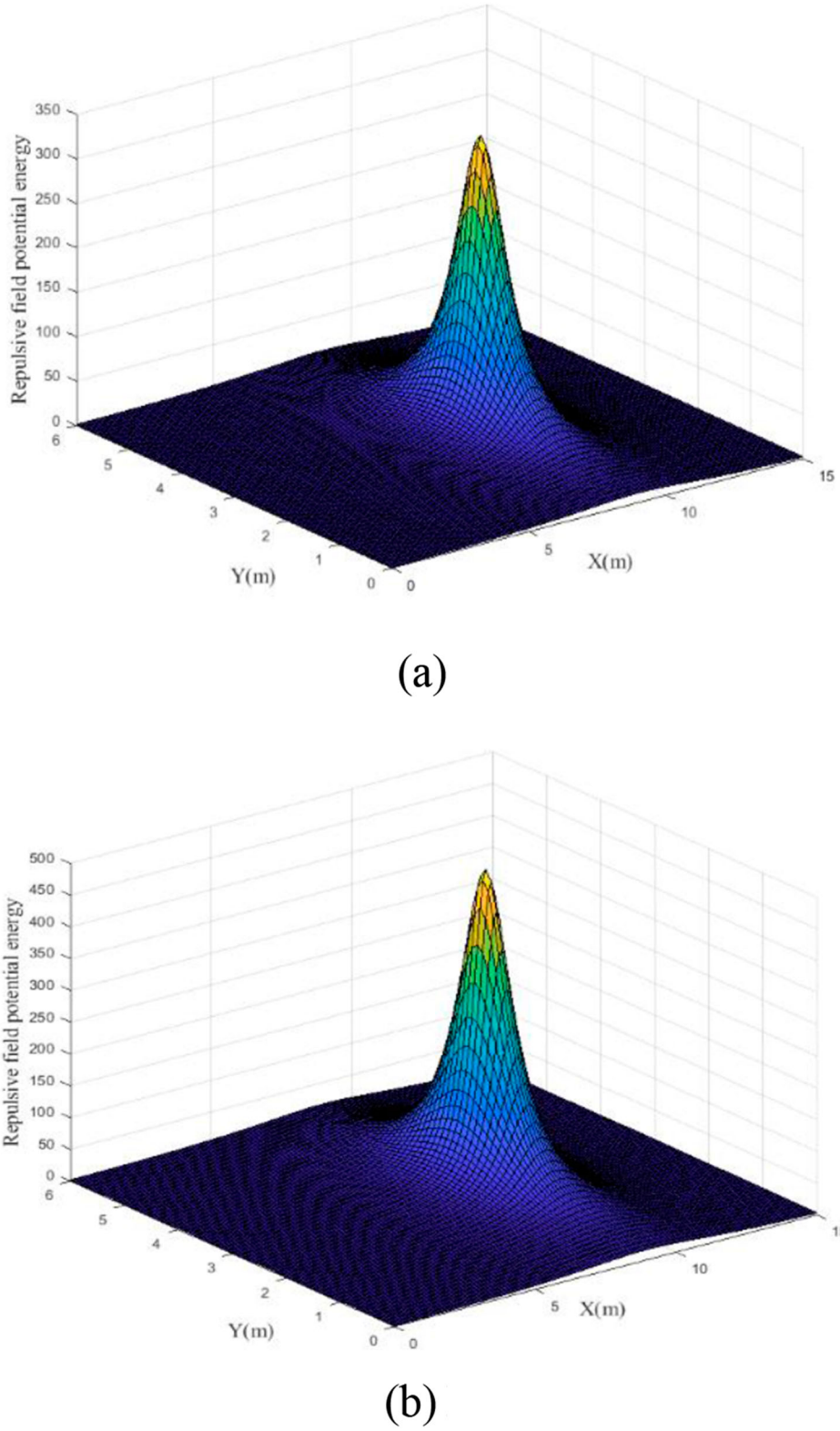

Figure 3. Repulsive field potential energy distribution map. (a) Relative speed 5 m/s. (b) Relative speed 10 m/s.

smooth, in line with the requirements of the actual driving process of the vehicle. Therefore, this paper uses a fifth-order polynomial to fit the local planning path:

$$Y_{\text{ref}} = \sum_{i=0}^{5} a_i t^i = a_0 + a_1 t + a_2 t^2 + a_3 t^3 + a_4 t^4 + a_5 t^5 \tag{18}$$

$$\varphi_{\text{ref}} = \sum_{i=0}^{5} b_i t^i = b_0 + b_1 t + b_2 t^2 + b_3 t^3 + b_4 t^4 + b_5 t^5 \tag{19}$$

where a_i, b_i are the coefficients of the two fitting polynomials, respectively.

At this point, a reference path for local path planning can be obtained, as shown in Figure 4.

2.4. Local speed planning

In the process of intelligent vehicle steering obstacle avoidance, if the smart car is still driving at the current speed, it will seriously affect the safety and ride comfort of the smart car when it is high-speed steering obstacle avoidance. The speed planning for the intelligent vehicle to avoid obstacles is to achieve vehicle safety, which is the basis for comfortable driving. Therefore, it is necessary to carry out the speed planning of the vehicle on the basis of the local path planning. In the case of the horizontal and vertical coordinated control, the intelligent vehicle can effectively avoid the obstacles smoothly.

Based on the obstacle avoidance path planning shown in Figure 4, considering the position and speed of the obstacle relative to the intelligent vehicle, a reference speed control model as shown in the following equation is established:

$$v_{\text{ref}} = \begin{cases} \lambda \dfrac{d}{v' t_d + \frac{v'^2}{2a_{\max}} + d_0} v', & d \le \rho_0 \\ v', & d > \rho_0 \end{cases} \tag{20}$$

where d is the relative distance between the intelligent vehicle and the obstacle; d_0 is the reserved safety distance; v' is the speed of the intelligent vehicle before the obstacle avoidance; $a_{\max}$ is the maximum deceleration of the intelligent vehicle; λ is a constant coefficient; t_d is the time from when the smart vehicle starts braking to when it stops. ρ_0 is the obstacle influence range (here, the obstacle influence range is a circle) (Figure 5).

It can be seen from the Equation (20) that after the intelligent vehicle enters the range of the obstacle, the speed can decrease as the distance from the obstacle decreases. When the vehicle bypasses the obstacle, the speed varies with the distance between the vehicle and the obstacle. When the intelligent vehicle drives out of the obstacle's range of influence, the vehicle speed will no longer be controlled by the model, thereby continuing to accelerate under the action of the gravitational force generated by the reference trajectory.

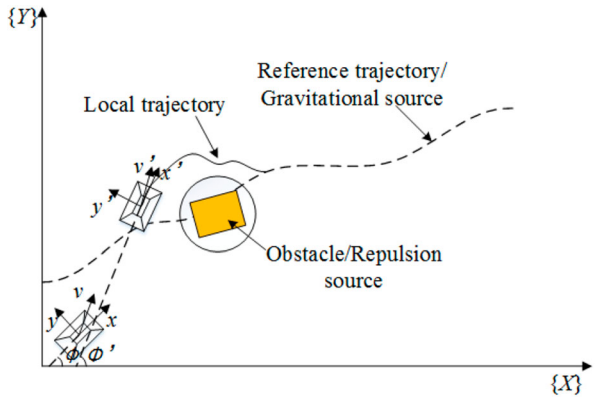

Figure 4. Obstacle avoidance path planning.

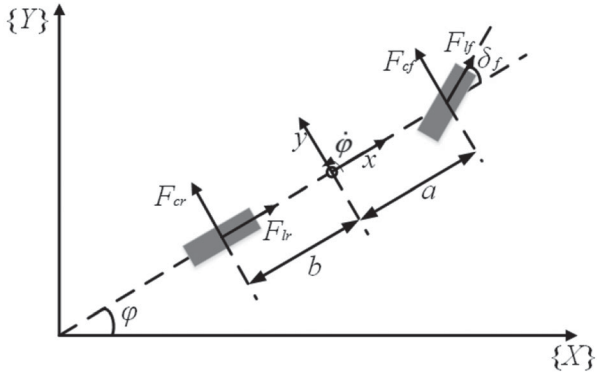

Figure 5. Simplified diagram of vehicle dynamics model.

3. Tracking controller design

3.1. Vehicle model

Before designing the model predictive controller, the three-degree-of-freedom vehicle dynamics model is first established. In the modelling process, considering the steering stability of the vehicle and the real-time performance of the controller, the following assumptions are made on the vehicle model: (1) it is ignored that, the smart vehicle is assumed on a flat road surface. In addition, the slope and other factors as well as the vertical motion of the vehicle are ignored; (2) assuming that the vehicle is a rigid body, the influence of the suspension system on the trajectory tracking is ignored; (3) considering the tire lateral deflection characteristics, the relationship between the longitudinal and lateral coupling of the tire is ignored; (4) using a planar motion vehicle model describing the motion of the vehicle, ignoring the left and right load transfer; (5) the resistance of the vehicle aerodynamics is ignored, and the three-degree-of-freedom vehicle dynamics model is shown in Figure 5.

According to the simplified model of the vehicle dynamics model, the vehicle dynamics differential equations are obtained by Newton's second law:

$$\begin{aligned} ma_y &= -mv_x\dot{\varphi} + 2F_{\text{lf}}\cos\delta_f - 2F_{\text{cf}}\sin\delta_f + 2F_{\text{lr}} \\ ma_x &= mv_y\dot{\varphi} + 2F_{\text{lf}}\sin\delta_f + 2F_{\text{cf}}\cos\delta_f + 2F_{\text{cr}} \\ \dot{\varphi} &= \omega \\ I_z\dot{\omega} &= 2a(F_{\text{lf}}\sin\delta_f + F_{\text{cf}}\cos\delta_f) - 2bF_{\text{cr}} \end{aligned} \tag{21}$$

The conversion relationship between the body coordinate system and the geodetic coordinate system is

$$\begin{aligned} \dot{X} &= v_x\cos\varphi - v_y\sin\varphi \\ \dot{Y} &= v_x\sin\varphi + v_y\cos\varphi \end{aligned} \tag{22}$$

Assuming the vehicle is front wheel steering, and based on the side yaw angle and the longitudinal slip ratio is small, the tire force can be approximated by a

linear function:

$$\begin{aligned} F_{\mathrm{lf}} &= C_{\mathrm{lf}} s_f \\ F_{\mathrm{lr}} &= C_{\mathrm{lr}} s_r \\ F_{\mathrm{cf}} &= C_{\mathrm{cf}} \alpha_f \\ F_{\mathrm{cr}} &= C_{\mathrm{cr}} \alpha_r \end{aligned} \tag{23}$$

Based on the small angle assumption, the side angle is calculated as follows:

$$\begin{aligned} \beta &= \frac{\dot{y}}{\dot{x}} \\ \alpha_f &= \beta + \frac{a\dot{\varphi}}{\dot{x}} - \delta_f \\ \alpha_r &= \beta - \frac{b\dot{\varphi}}{\dot{x}} \end{aligned} \tag{24}$$

In summary, the dynamic model of the available vehicle is

$$\begin{aligned} \dot{X} &= v_x \cos\varphi - v_y \sin\varphi \\ \dot{Y} &= v_x \sin\varphi + v_y \cos\varphi \\ \dot{\varphi} &= \omega \\ \dot{v}_x &= a_x \\ \dot{v}_y &= A_1 \omega + B_1 v_y + C_1 \delta_f \\ \dot{\omega} &= A_2 \omega + B_2 v_y + C_2 \delta_f \end{aligned} \tag{25}$$

Among them:

$$\begin{aligned} A_1 &= -v_x + \frac{2bC_{\mathrm{cr}} - 2aC_{\mathrm{cf}}}{mv_x}, \\ A_2 &= -\frac{2a^2 C_{\mathrm{cf}} + 2b^2 C_{\mathrm{cr}}}{I_z v_x}, \\ B_1 &= -\frac{2C_{\mathrm{cr}} + 2C_{\mathrm{cf}}}{mv_x}, \\ B_2 &= \frac{2bC_{\mathrm{cr}} - 2aC_{\mathrm{cf}}}{I_z v_x}, C_1 = \frac{2C_{\mathrm{cf}}}{m}, \\ C_2 &= \frac{2aC_{\mathrm{cf}}}{m} \end{aligned}$$

According to the state space system, select state variables $\boldsymbol{\xi} = \begin{bmatrix} v_y & v_x & \varphi & \omega & Y & X \end{bmatrix}^{\mathrm{T}}$, control input $\boldsymbol{u} = \begin{bmatrix} \delta_f & a_x \end{bmatrix}^{\mathrm{T}}$, control output $\boldsymbol{\eta} = \begin{bmatrix} Y & \varphi & \dot{x} \end{bmatrix}^{\mathrm{T}}$, the equation of state of the vehicle dynamics model is

$$\begin{aligned} \dot{\boldsymbol{\xi}} &= f(\boldsymbol{\xi}, \boldsymbol{u}) \\ \boldsymbol{\eta} &= g(\boldsymbol{\xi}) \end{aligned} \tag{26}$$

3.2. Model predictive controller design

Based on the vehicle dynamics model presented in Section 2.1, the predictive model of the trajectory tracking model predictive controller is established. Its main function is to use the historical information of the object and obtain control input sequence to predict the future output of the system. The vehicle dynamics model is linearized and discretized in the same way as in Section 1.1 to obtain a discretized prediction model:

$$\begin{aligned} \tilde{\boldsymbol{\xi}}(k+1) &= \tilde{\boldsymbol{A}}_d \tilde{\boldsymbol{\xi}}(k) + \tilde{\boldsymbol{B}}_d \tilde{\boldsymbol{u}}(k) \\ \tilde{\boldsymbol{\eta}}(k) &= \tilde{\boldsymbol{C}}_d \tilde{\boldsymbol{\xi}}(k) \end{aligned} \tag{27}$$

In the process of considering path tracking and vehicle speed tracking, the deviation between the actual path and the reference path should be made as small as possible, so that the actual vehicle speed is as close as possible to the reference vehicle speed. It is also necessary to ensure that the control input gain is as small as possible and from literature [19] defines the optimization objective function:

$$\begin{aligned} &\boldsymbol{J}(\boldsymbol{\xi}(t), \boldsymbol{u}(t-1), \Delta\boldsymbol{u}(t)) \\ &= \sum_{i=1}^{N_p} ||\boldsymbol{\eta}(t+i|t) - \boldsymbol{\eta}_{\mathrm{ref}}(t+i|t)||_{\boldsymbol{Q}}^2 \\ &\quad + \sum_{i=1}^{N_c-1} ||\Delta\boldsymbol{u}(t+i|t)||_{\boldsymbol{R}}^2 + \rho\varepsilon_r^2 \end{aligned} \tag{28}$$

where the first term is the difference between the actual vehicle speed and the reference vehicle speed; the second term is the control input increment; Q and R are the weight matrix; ρ is the weight coefficient of ε_r, when the system tracks. When the error is small, a larger value is taken to ensure that the intelligent vehicle can stabilize the error-free tracking path. When the tracking error is large, a small value to improve the safety of the vehicle is taken [20].

Table 1. Vehicle parameters.

Parameter	Parameter value
Vehicle mass m	1723 kg
Moment of inertia of the vehicle around the z-axis I_z	4175 kg m^2
Distance from the front axle of the vehicle to the centre of mass a	1.204 m
Distance from the rear axle of the vehicle to the centre of mass b	1.268 m
Front wheel cornering stiffness c_{cf}	66,900 N rad^{-1}
Rear wheel cornering stiffness c_{cr}	62,700 N rad^{-1}
Tire slip ratio s_f, s_r	0.2
Rolling resistance coefficient f_r	0.02

Table 2. Controller parameters.

Parameter	Planning controller	Tracking controller
Sampling time T	0.1 s	0.05 s
Predicted time domain N_p	15	10
Control time domain N_c	6	3
Weight coefficient Q_η	100	–
Weight coefficient R_u	50	–
Weight coefficient S_{obs}	10	–
Output weight matrix Q	–	[100, 0, 0; 0, 100, 0; 0, 0, 100]
Control weight matrix R	–	50,000
Correction factor ε	0.2	–
Relaxation factor ε_r	–	10
Relaxation factor weight coefficient ρ	–	1000

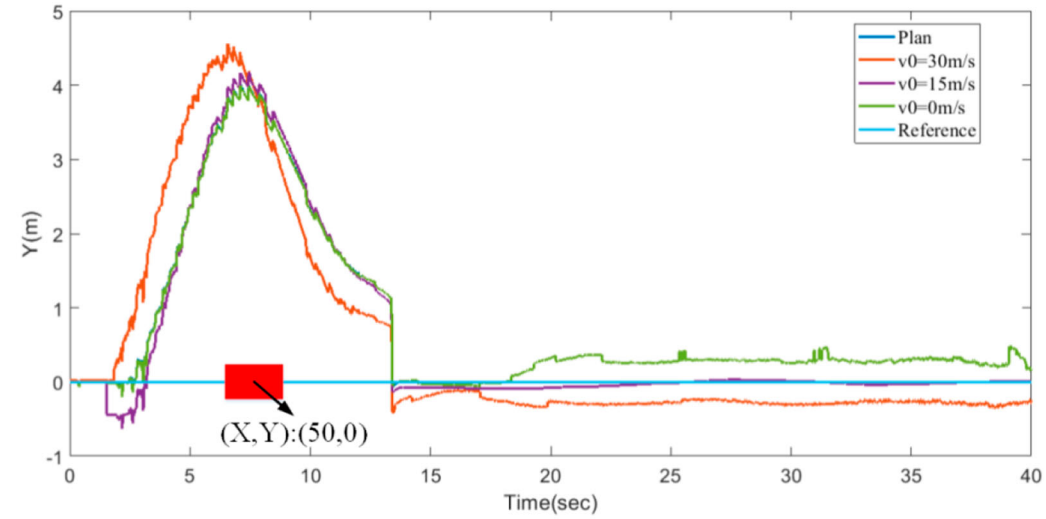

(a)

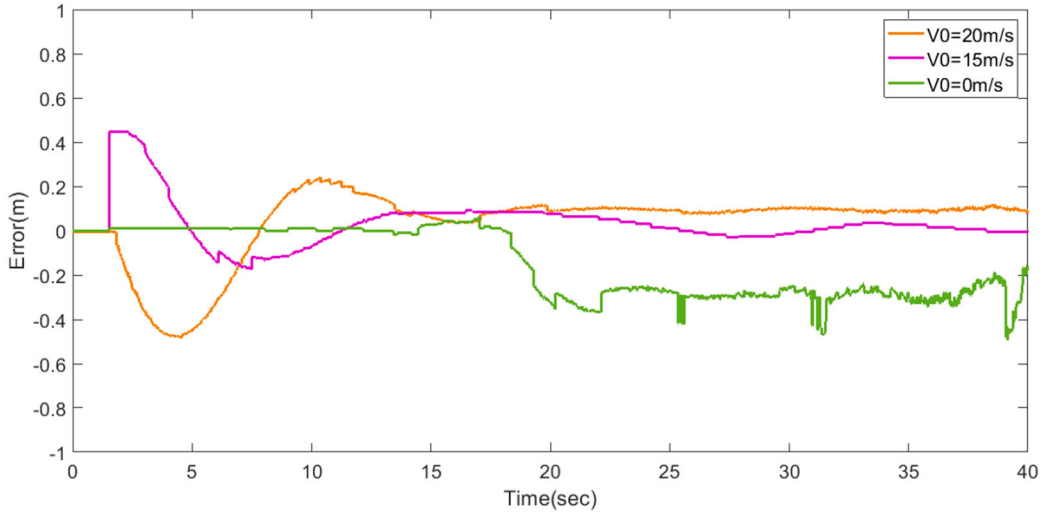

(b)

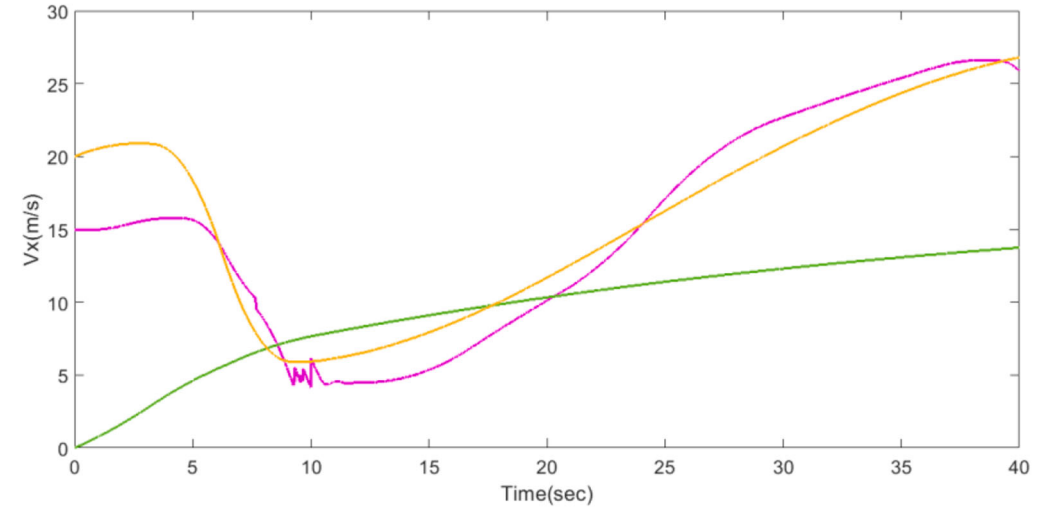

(c)

Figure 6. Static obstacle avoidance accuracy simulation results. (a) Lateral position. (b) Lateral positional deviation. (c) Vertical speed.

The above formula can be easily converted into a standard quadratic form for easy solution, and the control increment and relaxation factors in the equation can prevent the occurrence of infeasible results during the solution [21]. However, since the magnitude of control in the objective function appears as a control increment, the constraint must also appear as a control increment.

For the design of constraints, firstly, considering the constraints of control quantity and control increment in the control process, the longitudinal acceleration is generally −0.9–0.6 g, and the rate of change is generally −2–2 g/s. In addition, the front wheel angle is generally between −10° and 10°, and the rate of change is generally −9.4–9.4°/s [22].

Secondly, considering the vehicle running on a road with a low adhesion coefficient, it is necessary to ensure the stability of the operation. The reason why the vehicle will be unstable under the extreme working conditions is mainly because the tire force generated and the saturated ground. Vehicle centroid angle β or yaw rate ω is one of the key parameters to measure vehicle stability. To simplify the solution, the yaw rate ω is constrained to meet the stability requirements of the vehicle. In summary, the trajectory tracking problem can be transformed into an optimization problem as described below:

$$\begin{aligned} &\min_{\Delta \boldsymbol{u}(t)} \boldsymbol{J}(\boldsymbol{\xi}(t), \boldsymbol{u}(t-1), \Delta \boldsymbol{u}(t)) \\ &\text{s.t. } \boldsymbol{u}_{\min} \le \boldsymbol{u} \le \boldsymbol{u}_{\max} \\ &\Delta \boldsymbol{u}_{\min} \le \Delta \boldsymbol{u} \le \Delta \boldsymbol{u}_{\max} \\ &\boldsymbol{\eta}_{\min} \le \boldsymbol{\eta} \le \boldsymbol{\eta}_{\max} \\ &\omega_{\min} \le \omega \le \omega_{\max} \end{aligned} \tag{29}$$

The solution is completed in each control cycle, and a series of control increment sequences in the control time domain are obtained, and the first element of the sequence is applied to the system as the actual control volume, thereby solving the reciprocating cycle.

4. Simulation analysis

4.1. Simulation conditions and major parameters

In order to verify the effectiveness of the proposed collision avoidance control method, the CarSim and

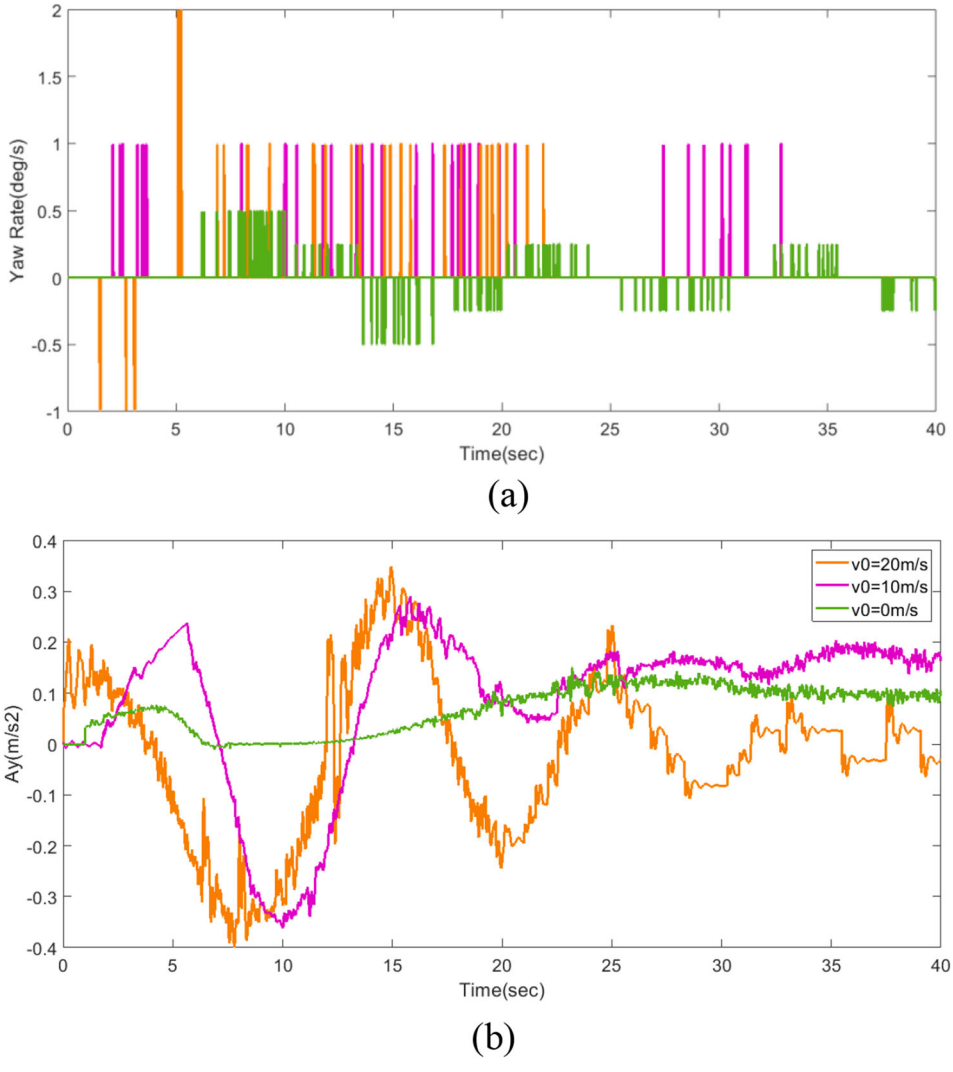

Figure 7. Static obstacle avoidance stability simulation results. (a) Yaw angle. (b) Lateral acceleration.

Matlab/Simulink co-simulation platform was built, and the C-Class car in CarSim was selected as the test vehicle. The main parameters are shown in Table 1. Assuming that the vehicle is under high road conditions, i.e. $\mu = 0.85$, so that the vehicle is at different initial vehicle speeds $v_0 = 0$ m/s, $v_0 = 15$ m/s, $v_0 = 20$ m/s, obstacle speed. When $v_p = 0$ m/s and $v_p = 10$ m/s, the simulation analysis of obstacle avoidance performance is carried out, and the corresponding controller parameters are shown in Table 2.

4.2. Analysis of simulation results

4.2.1. Static obstacle avoidance

For the condition that the reference path is a straight line, the static obstacle avoidance performance of the

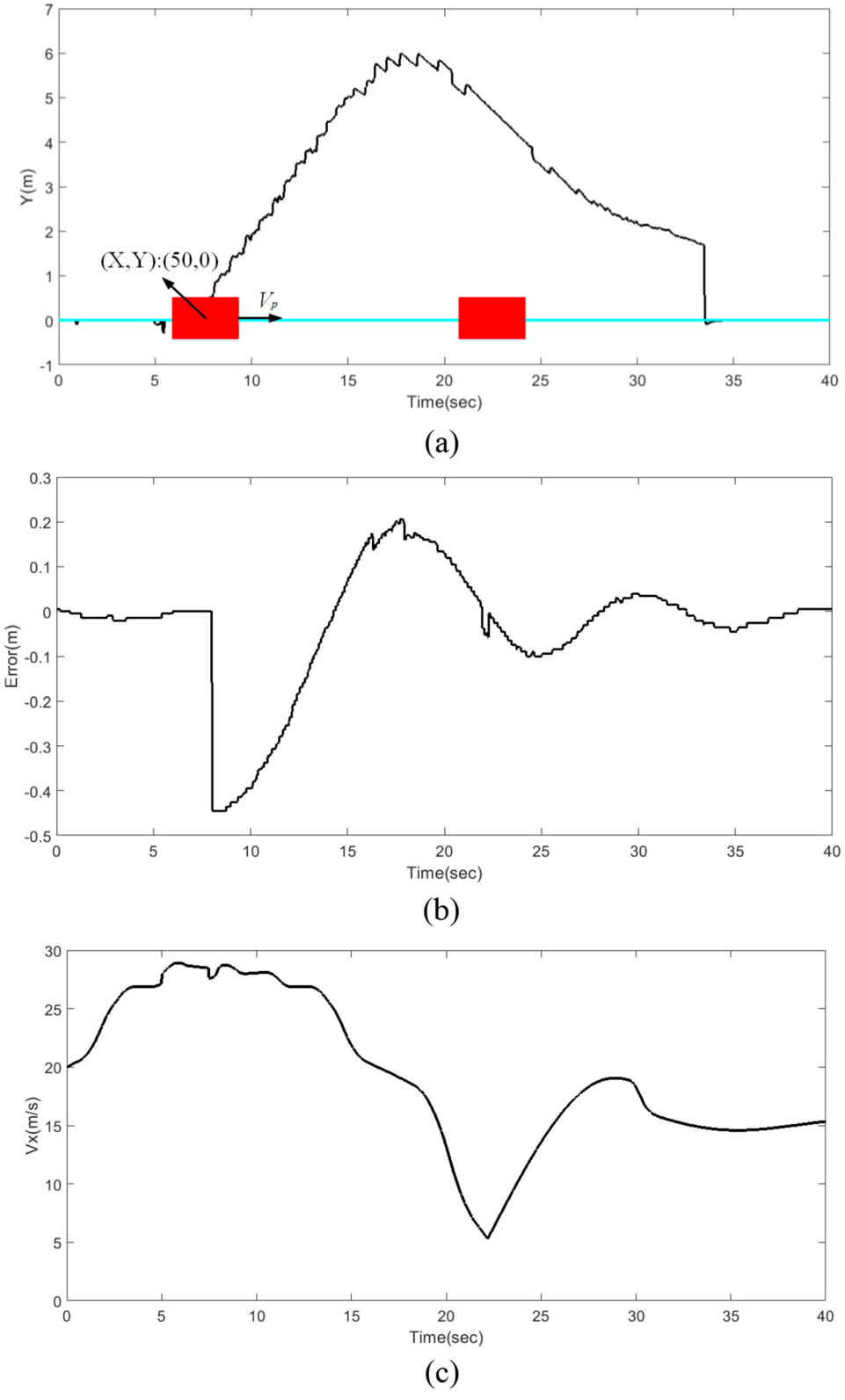

Figure 8. Dynamic obstacle avoidance accuracy simulation results. (a) Lateral position. (b) Lateral positional deviation. (c) Longitudinal speed.

intelligent vehicle is simulated and analysed. When the obstacle velocity $v_p = 0$ m/s, the obstacle is in a static state, and the coordinate position is (50 m, 0 m). The intelligent vehicle starts from the initial position (0 m, 0 m) at different initial speeds. In the active obstacle avoidance process, the lateral position, lateral position deviation and longitudinal speed simulation results representing the obstacle avoidance accuracy which are shown in Figure 6. The lateral acceleration and yaw rate simulation results representing the stability of the intelligent vehicle are shown in Figure 7.

It can be seen from Figure 6 that the obstacle avoidance controller can effectively realize the obstacle avoidance function. When the initial vehicle speed of the intelligent vehicle is high, the time for starting the active obstacle avoidance is earlier than that of the initial vehicle speed or the initial stationary state. Avoiding the obstacle error is relatively large; irrespective of how large the initial vehicle speed is, the speed of the intelligent vehicle gradually decreases in the process of approaching the obstacle. After the obstacle avoidance is completed, the intelligent vehicle gradually accelerates under the action of the obstacle repulsive field, and the vehicle exits the obstacle. After the range of action, the speed of the vehicle tends to be flat.

As shown in Figure 7, in the active obstacle avoidance process, although the initial yaw speed is higher, the yaw angular velocity and lateral acceleration of the vehicle fluctuate greatly, but it is relatively flat and is within the bound range. Vehicle handling stability and ride comfort of the vehicle.

4.2.2. Dynamic obstacle avoidance

It can be seen from the above static obstacle avoidance simulation results that even if the initial vehicle speed is low, the intelligent vehicle first speeds up, and the vehicle speed is gradually reduced after reaching the range of the obstacle, so this paper analyses the dynamic obstacle avoidance situation of the intelligent vehicle. The initial vehicle speed $v_0 = 20$ m/s, the obstacle velocity $v_p = 10$ m/s, the simulation results are shown in Figure 8 and Figure 9.

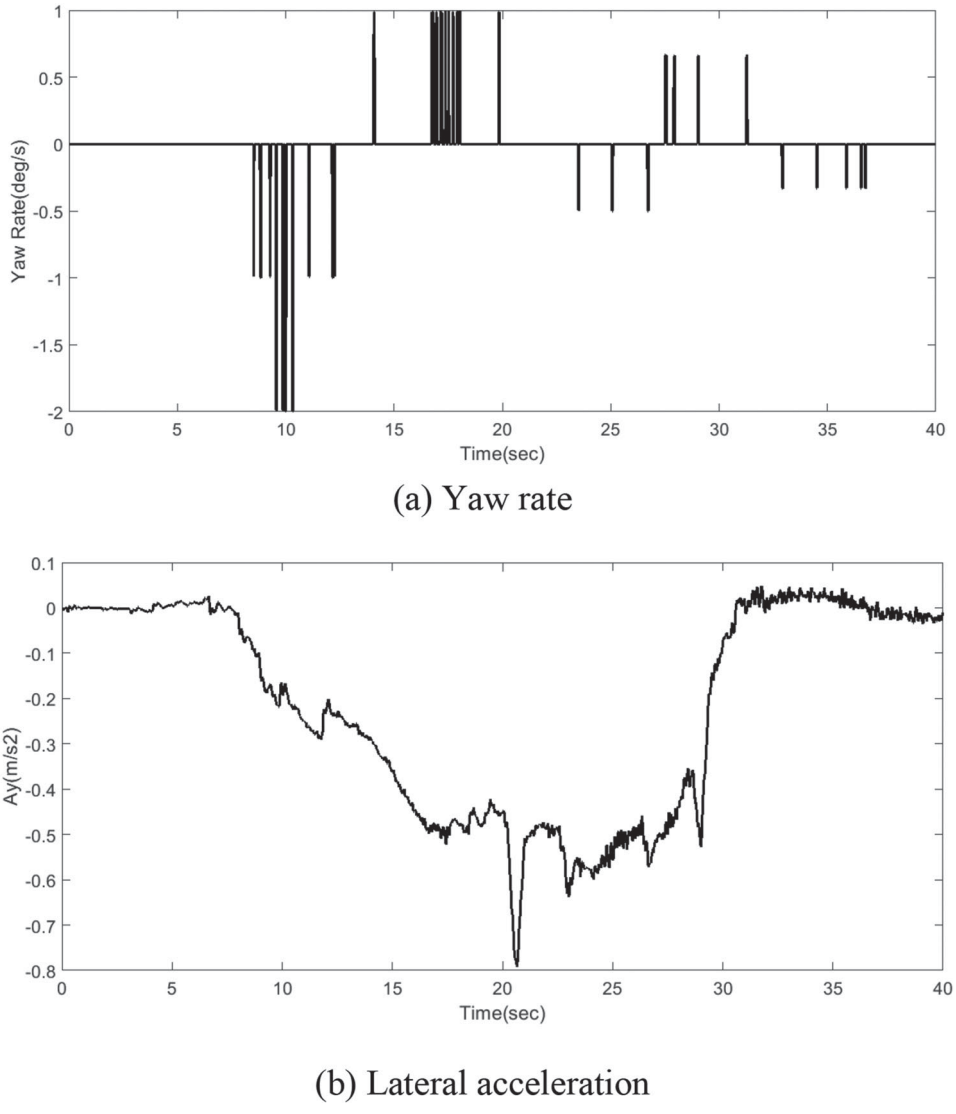

Figure 9. Dynamic obstacle avoidance stability simulation results. (a) Yaw rate. (b) Lateral acceleration.

It can be seen from Figure 8 and Figure 9 that under the condition that the obstacle travels in the same direction as the intelligent vehicle at a speed of 10 m/s, the intelligent vehicle can effectively achieve obstacle avoidance (here, it can also be used as overtaking, that is, the obstacle is an obstacle vehicle). It can be seen from Figure 8(a) the lateral position curve of the intelligent vehicle that although the effective obstacle avoidance can be realized, the safety distance of the intelligent vehicle for avoiding the obstacle of the dynamic obstacle is too large, so that the running cost of the vehicle becomes high, and thus, further optimize the planning control method. In addition, the yaw rate and the lateral acceleration, which represent the stability of the intelligent vehicle, are all within the constraint range, which ensures the stability of the vehicle and the ride comfort.

5. Conclusions

Aiming at the problem of active obstacle avoidance of intelligent vehicles, a comprehensive path planning, speed planning and path tracking, and speed tracking control methods based on model predictive control theory are proposed. The reference trajectory gravitational field function and the obstacle repulsion field function are constructed by artificial potential field theory. Considering the position and velocity of the obstacle relative to the intelligent vehicle, the reference speed control model of the intelligent vehicle is established and introduced into the optimization objective function of the model predictive control. In addition, to realize the integrated planning of path and speed; designing the tracking controller of reference path and reference speed to realize the horizontal and vertical integrated control of intelligent vehicles. In this paper, co-simulation is carried out on CarSim and Matlab/Simulink platform, and the simulation verification of the proposed active obstacle avoidance control method is accomplished.

The simulation results show that the model predictive control planning layer based on the kinematics model can plan the local obstacle avoidance path in real-time and accurately according to the state information of the intelligent vehicle and the relative motion information of the obstacle. The reference speed is designed in the obstacle avoidance process. The control model can generate the appropriate reference speed; the model predictive control tracking layer based on the dynamic model can accurately predict the future state of the vehicle and optimize the optimal front wheel angle and longitudinal acceleration to realize the horizontal and vertical integrated control of the intelligent vehicle, which not only guarantees The accuracy of the reference trajectory tracking also ensures the safety and ride comfort of the vehicle.

In this paper, only the horizontal and vertical integrated control strategies of the active obstacle avoidance of intelligent vehicles with obstacles in constant driving state are simulated. Under actual circumstances, the obstacles will be in multiple driving states, which will cause complex decision planning for intelligent vehicles. Therefore, it is necessary to further improve the control method and improve its applicability to the real environment.

Disclosure statement

No potential conflict of interest was reported by the author(s).

References

[1] Rosolia U, De Bruyne S, Alleyne AG. Autonomous vehicle control: a nonconvex approach for obstacle avoidance. IEEE Trans Control Syst Technol. 2016;25(2):469–484.
[2] Zhu M, Chen H, Xiong G. A model predictive speed tracking control approach for autonomous ground vehicles. Mech Syst Signal Process. 2017;87:138–152.
[3] Li L, Lu Y, Wang R, et al. A three-dimensional dynamics control framework of vehicle lateral stability and rollover prevention via active braking with MPC. IEEE Trans Ind Electron. 2016;64(4):3389–3401.
[4] Douthwaite JA, Zhao S, Mihaylova LS. Velocity obstacle approaches for multi-agent collision avoidance. Unmanned Syst. 2019;7(01):55–64.
[5] Sabry Y, Aly M, Oraby W, et al. Fuzzy control of autonomous intelligent vehicles for collision avoidance using integrated dynamics. SAE Int J Passeng Cars-Mech Syst. 2018;11:5–21.
[6] Kim YH, Park JB, Yoon TS. Modified turn algorithm based ground vehicle collision avoidance. Electron Lett. 2018;54(9):558–560.
[7] Choe TS, Hur JW, Chae JS, et al. Real-time collision avoidance method for unmanned ground vehicle. In: 2008 International Conference on Control, Automation and Systems. IEEE; 2008. p. 843–846.
[8] Moon S, Lee U, Shim DH. Study on real-time obstacle avoidance for unmanned ground vehicles. In: ICCAS 2010. IEEE; 2010. p. 1332–1335.
[9] Tomas-Gabarron JB, Egea-Lopez E, Garcia-Haro J. Vehicular trajectory optimization for cooperative collision avoidance at high speeds. IEEE Trans Intell Transp Syst. 2013;14(4):1930–1941.
[10] Wang J, Wu J, Li Y. The driving safety field based on driver–vehicle–road interactions. IEEE Trans Intell Transp Syst. 2015;16(4):2203–2214.
[11] Cao H, Song X, Huang Z, et al. Simulation research on emergency path planning of an active collision avoidance system combined with longitudinal control for an autonomous vehicle. Proc Inst Mech Eng D J Automob Eng. 2016;230(12):1624–1653.
[12] Mousavi MA, Heshmati Z, Moshiri B. LTV-MPC based path planning of an autonomous vehicle via convex optimization. 2013 21st Iranian Conference on Electrical Engineering (ICEE). IEEE; 2013. p. 1–7.
[13] Rosolia U, De Bruyne S, Alleyne AG. Autonomous vehicle control: a nonconvex approach for obstacle avoidance. IEEE Trans Control Syst Technol. 2016;25(2):469–484.
[14] Ji J, Khajepour A, Melek WW, et al. Path planning and tracking for vehicle collision avoidance based on model predictive control with multiconstraints. IEEE Trans Veh Technol. 2016;66(2):952–964.

[15] Zhu M, Chen H, Xiong G. A model predictive speed tracking control approach for autonomous ground vehicles. Mech Syst Signal Process. 2017;87:138–152.
[16] Huang Z, Wu Q, Ma J, et al. An APF and MPC combined collaborative driving controller using vehicular communication technologies. Chaos Solit Fractals. 2016;89:232–242.
[17] Zhu X, Liu Z, Li L. Steering collision avoidance control strategy based on dangerous conditions of vehicles and pedestrians. J Automob Saf Energy Sav. 2015;6(3):217–223.
[18] Ren Y, Zheng L, Zhang W, et al. Research on active collision avoidance control of intelligent vehicle based on model predictive control. Automot Eng. 2019;41(4):404–410.
[19] Li S, Wang J, Li K. Stability method of soft constrained linear model predictive control system. J Tsinghua Univ Nat Sci Ed. 2010;11:1848–1852.
[20] Luo Y, Chen T, Li K. Nonlinear model predictive cruise control of hybrid electric vehicle. J Mech Eng. 2015;51(16):11–21.
[21] Wang Y, Cai Y, Chen L, et al. Design of intelligent Networked vehicle path tracking controller based on model predictive control. J Mech Eng. 2019;55(8):136–144+153.
[22] Xu Y, Lu L, Chu D, et al. A unified modeling method for trajectory planning and tracking control of unmanned vehicles. J Autom. 2019;45(4):799–807.